Journal of The Electrochemical Society, **146** (2) 600-606 (1999)
S0013-4651(97)10-113-6 CCC: $7.00

An In Situ X-Ray Absorption Spectroscopy Investigation of the Effect of Sn Additions to Carbon-Supported Pt Electrocatalysts
Part I

Sanjeev Mukerjee* and James McBreen*

Brookhaven National Laboratory, Department of Applied Science, Upton, New York 11973, USA

Carbon-supported platinum (Pt/C) with an adsorbed layer of underpotential deposited (upd) Sn is a much better catalyst for the methanol oxidation reaction (MOR) than a carbon-supported platinum-tin (PtSn/C) alloy. In situ X-ray absorption (XAS) was used to determine the differences in the effects that the two methods of Sn addition have on the electronic properties and the structural properties of the catalyst. X-ray diffraction and XAS at the Pt L_3 and L_2 edges indicate that the PtSn/C catalyst has a Pt_3Sn $L1_2$ structure, and alloying with Sn causes partial filling of the Pt d band vacancies and an increase in the Pt–Pt bond distance from 2.77 to 2.8 Å. However, upd Sn does not perturb Pt structurally or electronically. XAS at the Sn K edge indicates that both the upd Sn on Pt/C and the surface Sn on PtSn/C are associated with oxygenated species at all potentials, and that the nature and strength of the Sn–O bonds are potential dependent. The differences in the activity of the two catalysts for the MOR are due to the effects of alloying on the Pt electronic structure that inhibit the ability of the Pt to adsorb methanol and dissociate C–H bonds. The ability of PtSn/C to adsorb oxygen at low potentials enhances its activity for CO oxidation.

Manuscript submitted October 30, 1997; revised manuscript received October 8, 1998.

The electrocatalytic effect of adding Sn to Pt has been studied for its ability to enhance the electro-oxidation of methanol, CO, and other C_1 compounds, and its potential use in fuel cells. Early work on these electrocatalysts has been reviewed by McNicol.[1,2] Léger and Lamy.[3] Parsons and Vandernoot[4] have reviewed later work in the eighties. Most of the earlier papers[1,2,5-11] have reported that the presence of Sn enhances the activity for the methanol oxidation reaction (MOR) as compared to pure Pt. However, others[12-14] have reported activities which are only slightly higher than Pt. The source of these inconsistencies is the variety of methods used to add Sn to Pt, ranging from (*i*) electrochemical codeposition, (*ii*) underpotential deposition (upd) of Sn on Pt, and (*iii*) alloy formation, which effect the state of the bimetallic electrocatalyst. The majority of the reports related to enhancements in electrode kinetics involve electrocatalysts where Sn is not alloyed with Pt (such as upd deposition). Most of the studies related to bulk PtSn alloys, particularly the Pt_3Sn alloy phase[12,13] have reported little or no enhancements. In contrast, however, is a report of enhanced activity on carbon-supported PtSn alloy electrocatalysts containing primarily Pt_3Sn phase (the minor phase being PtSn).[15] Besides these inconsistencies, it has also been reported that Pt_3Sn bulk alloy exhibits enhanced activity for CO electro-oxidation.[16] These enhancements were reported to be higher than that found for PtRu alloys,[16] a bimetallic electrocatalyst which shows consistent enhancements for CO and methanol oxidation regardless of the mode of preparation (alloy, upd deposition, etc.). Hence the apparent paradox: PtSn alloy is a good electrocatalyst for CO electro-oxidation but apparently not for methanol, but upd Sn on Pt has been consistently reported for its enhanced activity for the MOR. In the case of both CO and methanol there is overwhelming evidence[3,4,17,18] of Pt surface poisoning with species such as CO and CHO. Mechanisms such as the "bifunctional mechanism"[19] can explain the role played by the more oxidizable second element in nucleating OH-type species at lower potentials and hence promoting methanol and CO electro-oxidation. However, it fails to explain the inconsistencies based on the differences in Pt–Sn interactions and the reasons for different activities for methanol and CO electro-oxidation.

In this investigation we have examined the effect of Sn additions to Pt both as an alloying element as well as a upd deposit in terms of its activity for the MOR. In order to resolve the paradoxical nature of these electrocatalysts, their electrochemical characteristics have been correlated with results from in situ X-ray absorption spectroscopy. X-ray absorption spectroscopy (XAS) offers the unique ability to simultaneously probe both the electronic and structural parameters under in situ electrochemical conditions with element specificity. The ability to probe the L_3 and L_2 absorption edges (p-d transitions) of Pt under in situ electrochemical conditions using the near edge part of the spectra (X-ray absorption near edge structure, XANES) provides a direct measure of Pt 5-d band vacancies/atom. In addition to this, both the Pt L and Sn K edge XANES spectra can provide information on the changes in the oxidation state, perturbation of the electronic states due to adsorption of OH, H, and C_1 species and corrosion/dissolution of the more oxidizable alloying element. The postedge region of the spectrum (50-1500 eV beyond the Pt L_3 edge) referred to as the extended X-ray absorption fine structure (EXAFS), provides information on the short range atomic order (bond distances, coordination numbers, etc.).

The efficacy of this technique in the study of electrocatalysis of oxygen reduction[20,21] and hydrogen oxidation[22] has been amply demonstrated before on a series of binary carbon supported alloys of Pt with first row transition elements. Further, there have been reports on XAS studies of PtRu/C [23] in $HClO_4$ and during CO oxidation.[24] Also, XAS has been used to elucidate the reasons for the decrease in specific activity of Pt/C for both O_2 reduction and methanol oxidation as the particle size is decreased.[25]

XAS has been used to study PtSn catalysts on oxide supports.[26-28] The early work of Meitzner et al. showed that a PtSn alloy was formed on a SiO_2 support.[26] Furthermore, they demonstrated that the contributions of Pt and Sn to the Pt coordination could easily be distinguished because of the large differences in the phase and amplitude functions for the two coordinating elements.

This investigation is presented in two parts. The first comprises of in situ XAS studies on carbon-supported Pt with and without upd Sn and a carbon-supported PtSn alloy at the Pt L and Sn K edges in 1 M $HClO_4$ electrolyte without the presence of C_1 moieties (CH_3OH, and CO). The second part will give the results on these catalysts in 1 M $HClO_4$ in the presence of 0.3 M CH_3OH and adsorbed CO.

Experimental

Electrodes, cells, electrochemical, and X-ray diffraction analysis.—Carbon-supported Pt and PtSn alloy electrocatalysts were procured from E-TEK Inc. (Framingham, MA). E-TEK specified a metallic loading of 20% on the carbon support (Vulcan XC-72, Cabot Corporation, USA). The specified Pt:Sn atomic composition was 3:1. UPD of Sn on carbon-supported Pt was carried out using a 3 mM $SnCl_4$ solution in either 1 M $HClO_4$ or 0.5 M H_2SO_4 and potentiostatically polarizing it at 330 mV vs. RHE for 3.75 h.

* Electrochemical Society Active Member.

S0013-4651(97)10-113-6 CCC: $7.00

X-ray powder diffraction analysis on the Pt/C and PtSn/C alloy electrocatalysts was carried out at beam line X27A in the National Synchrotron Light Source (NSLS). The samples were mounted in a transmission geometry on a two-circle goniometer and LiF <200> crystal was used as an analyzer. The X-ray energy was set at ~24.5 keV ($\lambda = 0.505$ Å). Details of the optics of this beam line and the diffraction analysis are given elsewhere.[29]

Electrodes were prepared using a standard vacuum table paper making technique.[23] The electrode composition was 76% carbon-supported catalyst, 12% carbon fiber, and 12% polytetrafluoreneethylene (PTFE) (T-30, Du Pont). The electrodes 19 mm diam, 0.08 g, and 0.6 mm thick were soaked for 24 h in 1 M $HClO_4$. This was done to eliminate any unreacted Sn since in the presence of Pt excess Sn will dissolve in $HClO_4$. In addition, it enabled the electrode to be completely wetted, an important criterion, since XAS in the transmission mode is a bulk-averaging technique.

Two types of spectroelectrochemical cells were used. The cell used for in situ studies on Pt/C and PtSn/C alloy in 1 M $HClO_4$ is described in detail elsewhere.[20,21,23] It comprised of a carbon foil counter electrode, a Nafion 117 (DuPont) membrane separator, a sealed reversible hydrogen reference electrode, and vent holes for the evolved gases. Each gasket in the spectroelectrochemical cell was sized 0.025 mm less than the corresponding component. This maintained all components under compression and prevented complications in the spectra due to random density fluctuations caused by formation of gas bubbles. The Nafion 117 membrane functioned primarily as a separator to prevent gas crossover. The cell used for the upd Sn on carbon-supported Pt has been described previously.[30] This cell had arrangements for electrolyte exchange and gas bubbling. These provisions enabled deposition of upd Sn on Pt/C under a N_2 atmosphere followed by exchange of electrolyte. So the Sn XAS spectra for the upd Sn could be recorded without complications from residual Sn(IV) ions in the electrolyte. Electrochemical control in all the electrochemical and in situ spectroelectrochemical studies was maintained using an EG&G PAR 273 (EG&G Princeton Applied Research) potentiostat/galvanostat interfaced with an IBM PS/2 computer.

XAS measurements.—The XAS measurements were done at beam lines X11A and X23A2 at the National Synchrotron Light Source (NSLS) with the storage ring operating at 2.58 GeV and an electron ring current of 110 to 350 mA. Details of the beam line configuration, monochromator design, resolution, detuning, etc., are given in previous publications.[20-23] In the case of Pt/C and PtSn/C alloy all measurements (Pt L and Sn K edges) were done in the transmission mode with a third detector and a metal foil reference for calibration and alignment of the spectra. XAS measurements of the Pt L edges for the upd Sn on Pt were done in the transmission mode using the same three-detector configuration for data acquisition as described above using 1 M $HClO_4$ electrolyte. The data at the Sn K edge was acquired separately in the fluorescence mode using 0.5 M H_2SO_4 electrolyte.

In the case of carbon-supported Pt, in situ XAS measurements were done at several potentials between 0.0 and 1.14 V [all potentials in this paper are with respect to the reversible hydrogen electrode (RHE)]. Most measurements were done between 0.0 and 0.84 V on both the PtSn/C alloy and the upd Sn on Pt/C. The lower upper limit was used to prevent dissolution of Sn and the formation of tetravalent Sn species. However, in separate electrochemical measurements and a few XAS experiments, more positive limits were sometimes used.

The methodology for the XANES data analysis followed the procedures described by Wong et al.[31] The methodology used to determine the Pt 5 d band vacancies are based on earlier work by Mansour and co-workers[32,33] and are described in detail elsewhere.[20-23] EXAFS analysis involved algorithms developed by Koningsberger and co-workers[34-36] and are described in detail elsewhere.[20-23] Detailed EXAFS analysis was carried out on the Pt L_3 edge data. Unique solutions for EXAFS parameters (bond distance, coordination numbers, etc.) were arrived at using nonlinear least square fitting[37] of the sample phase and amplitude parameters with those of standards derived either experimentally or through theoretical calculations. Standards for the Pt–Pt and Pt–O interactions involved phase and amplitude parameters derived experimentally from Pt foil and $Na_2Pt(OH)_6$, respectively, at liquid N_2 temperature. For the Pt–Sn interactions these parameters were derived from theoretical calculations using the FEFF program (version 5.1) of Rehr et al.[37] The corresponding parameters for the Sn-O interactions were derived experimentally from a SnO reference standard at liquid N_2 temperature. In the EXAFS analysis correlation effects between the coordination number (N) and the Debye-Waller factor ($\Delta\sigma^2$) and between bond distance (R) and potential shift (ΔE_0) were checked by comparing k^1 and k^3 weighted fits.[38]

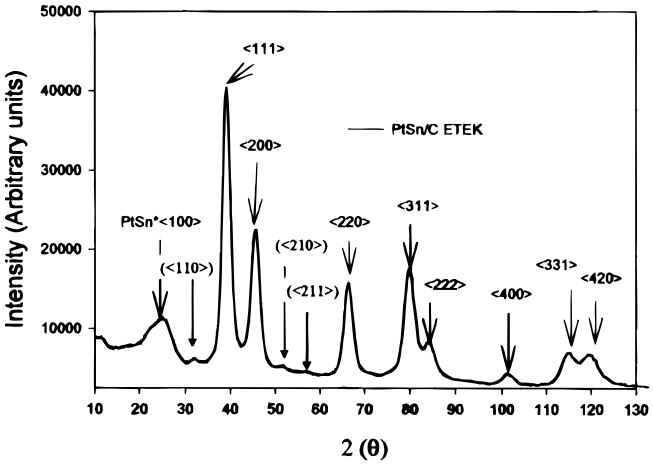

Figure 1. X-ray powder diffraction pattern for the as-received PtSn/C (E-TEK) alloy electrocatalyst. Data originally taken at $\lambda = 0.505$ is represented at the X-ray wavelength for Cu Kα. Superlattice lines have been indexed to an fcc lattice with *Pm*3*m* space group and a Pt_3Sn primary phase. some ordering in the superlattice is evident from the (*<110>), (<210>), and (<211>) diffraction lines.

Results and Discussion

X-Ray Diffraction and Electrochemical Characterization

Figure 1, shows the representative XRD pattern for the PtSn alloy electrocatalyst after conversion of 2θ positions to those for Cu Kα. The X-ray diffraction pattern is consistent with a fcc lattice with $L1_2$ structure of Pt_3Sn type stoichiometry.[39,40] The sharp lines are those associated with the fcc lattice and was indexed to a *Pm*3*m* space group. Some ordering of the lattice can be discerned by the diffraction lines from the superlattice as evidenced by the (<110>), (<210>), and (<211>) lines at 2θ positions of 31.6, 51, and 56.25°. Alloying of the Pt with Sn increases the lattice parameters (Table I), which differs from the lattice contraction seen with PtRu[23] and Pt alloyed with first row transition elements.[20,21] The particle size for the crystallites (Table I) was obtained using X-ray line broadening analysis by applying the Scherrer equation to the principle <111> diffraction line for the carbon supported Pt and PtSn alloy. The particle sizes were found to be in the range of 34-35 Å (Table I).

Table I. Results of X-ray powder diffraction and electrochemical characterization for Pt/C, PtSn/C, and upd Sn on Pt/C electrocatalysts.

Electrocatalyst	Lattice parameters (Pt–Pt bond distance) (Å)	Particle size (Å)
Pt/C	3.9271 (2.774)	32
PtSn/C	4.0015 (2.829)	34
UPD Sn on Pt/C	—	—

S0013-4651(97)10-113-6 CCC: $7.00

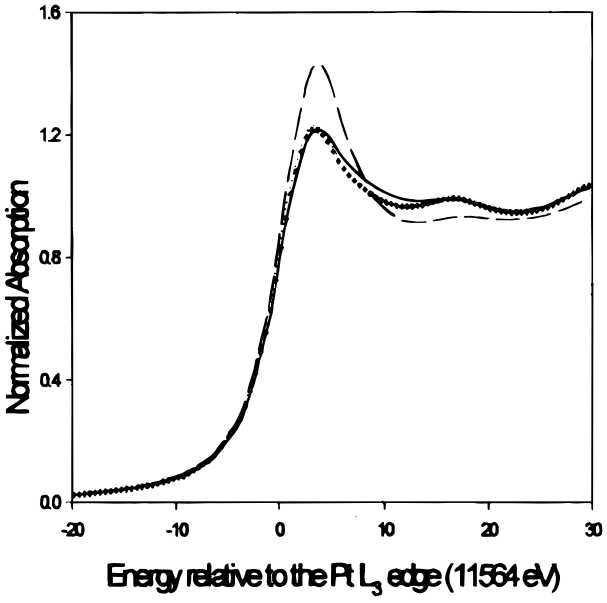

(a)

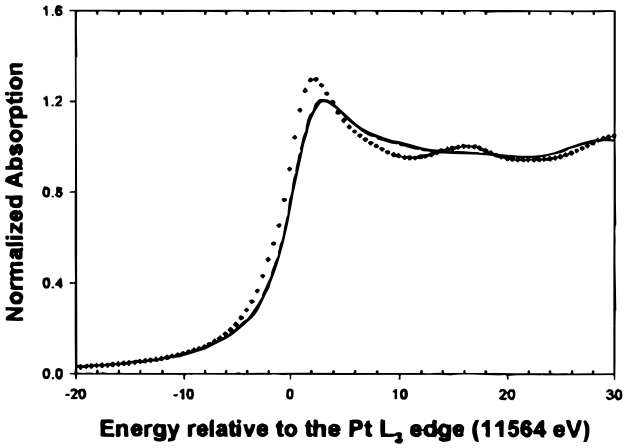

(b)

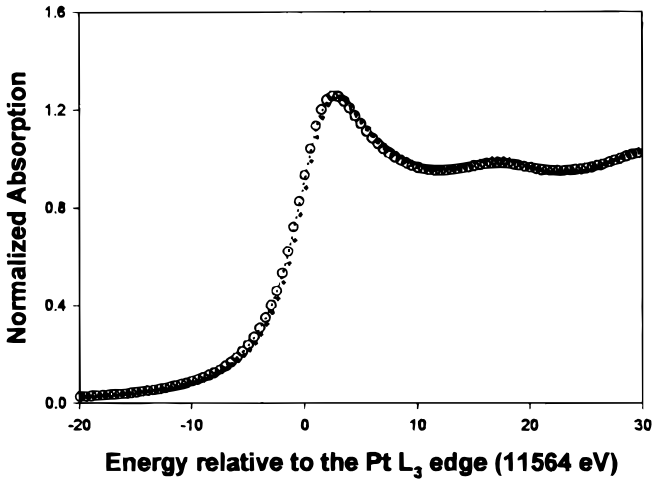

(c)

Figure 2. XANES spectra at the Pt L_3 edge in 1 M $HClO_4$ for (a) Pt/C, (b) PtSn/C alloy at 0.0 (—), 0.54 (····), and 0.84 V (---) vs. RHE, and (c) upd Sn on Pt/C at 0.33 (○), 0.54 V (····). Data for a Pt foil reference standard are also shown in each figure for comparison (+).

XAS Analysis

Analysis of the in situ XANES spectra for PtSn/C alloy in 1 M $HClO_4$ at 0.54 V at the Pt L_3 edges show step heights of 0.391 and 0.181, respectively, and that for Sn K edge under the same electrochemical conditions was 0.025. Using the absorption cross sections from the McMaster tables[41] the respective Pt and Sn loadings were calculated as 3.34 and 0.71 mg/cm^2. This gives a total Pt-Sn loading of 4.05 mg/cm^2, a value close to the 4.21 mg/cm^2 expected for the specified catalyst loading of 20%. The respective step heights yield an atomic ratio of Pt:Sn of 2.85:1, a value which agrees well with the Pt_3Sn stoichiometric phase exhibited by the XRD pattern and the specified composition of the alloy.

XAS at the Pt L_3 edge in 1 M $HClO_4$.—Pt XANES.—Figure 2a shows in situ XANES spectra at the Pt L_3 edge for Pt/C in 1 M $HClO_4$ at various potentials and for Pt foil. The magnitude of the normalized absorption intensity (white line) varies greatly with potential. The reasons for this have been described in detail elsewhere.[20-22] Briefly, the broadening of the white line at 0.0 V (hydrogen region) is attributed to the transition of electrons into unoccupied Pt–H antibonding orbitals. At 0.54 V, the white line is congruent to the foil due to lack of any anionic or other interactions on Pt electronic states. Above 0.8 V, coverage by an oxide layer causes emptying of the Pt 5 d band vacancies and a consequent increase in the white line. The calculated changes in the Pt 5 d band vacancies/atom are given in Table II. The XANES spectra for the PtSn/C alloy are given in Fig. 2b. As evident from the spectra, there is negligible effect of potential on the white line intensities, in contrast to Pt/C (similar particle size and carbon support). There is, however, a lowering of the white line intensity for the PtSn alloy as compared to the Pt foil, which indicates a filling of the Pt 5 d bands as a result of alloying with Sn. A similar lowering of the L_3 white line was observed for PtSn supported on SiO_2. [26] The Pt 5 d band vacancies/atom at 0.54 V gives an estimate of this filling (Table II). This effect of filling of the Pt 5 d band vacancies is opposite to that found for Pt alloyed with transition elements such as the first row transition metals ranging from Cr to Ni [20,21] and for Ru.[23] The absence of any perturbations with potential for the PtSn/C electrocatalyst, however, is similar to those observed for binary Pt alloys with the first row transition metals[20,21] and with Ru.[23] Figure 2c shows the Pt L_3 edge XANES for Pt/C with upd Sn on the surface. The spectra in the double-layer region are close to those for a Pt foil and are identical to those found for Pt/C, indicating minimal changes in the d band vacancies on the adsorption of Sn species. These spectra are averaged over the bulk of the crystallites and are not exclusive to the surface. However, in a 35 Å particle ~30% of the total atoms are surface atoms,[42] so XAS can easily detect effects due to adsorption of H, and OH species on the surface as can be seen from Fig. 2a.

S0013-4651(97)10-113-6 CCC: $7.00

Table II. Results of XANES and EXAFS analysis at the Pt L_3 edge for Pt/C and PtSn/C alloy electrocatalyst at 0.0, 0.54, and 0.84 V vs. RHE in 1 M $HClO_4$.

Pt/C Electrode potential (V)	Pt 5 d band vacancy/atom	Shell	EXAFS parameters N	R (Å)	$\Delta\sigma^2$ (Å^2)	ΔE_o (eV)
0.0	0.335	Pt–Pt	10.64	2.77	0.0044	0.93
0.54	0.329	Pt–Pt	8.66	2.77	0.0044	−0.88
0.84	0.370	Pt–Pt	6.73	2.77	0.0048	−0.20
		Pt–O	1.69	2.04	0.0042	2.48
PtSn/C Electrode potential (V)	**Pt 5 d band vacancy/atom**	**Shell**	**EXAFS parameters N**	**R (Å)**	**$\Delta\sigma^2$ (Å^2)**	**ΔE_o (eV)**
0.0	0.298	Pt–Pt	8.24	2.80	0.0055	2.91
		Pt–Sn	2.56	2.80	0.0132	−5.75
0.54	0.296	Pt–Pt	7.89	2.80	0.0051	3.55
		Pt–Sn	2.83	2.80	0.0097	−5.63
0.84	0.297	Pt–Pt	7.88	2.79	0.0052	4.20
		Pt–Sn	2.89	2.79	0.0089	−5.244

Pt EXAFS.—Figure 3 shows an in situ Pt L_3 edge EXAFS spectrum for PtSn/C alloy at 0.0 V in 1 M $HClO_4$ as a representative plot. The data quality, in the k range of 2.2 to 17 Å^{-1}, was excellent. The spectra for the Pt/C and with and without upd Sn were of similar high quality. The forward Fourier transforms of the EXAFS spectra for Pt/C and PtSn/C alloy at various potentials are given in Fig. 4. The windows used to obtain these forward Fourier transforms are given in Table III. The data for Pt/C (Fig. 4a) shows, significant changes in the Fourier transform as a function of potential. these have been explained in detail previously.[20-23] In contrast, the Pt EXAFS for the PtSn/C alloy shows no variations in the Pt L_3 edge Fourier transforms as a function of potential (Fig. 4b) This was evident from the Fourier transforms at 0.0, 0.54, and 0.75 V (not shown). In a separate experiment, the potential was allowed to exceed 0.85 to 1.0 V, where first signs of change in the Fourier transforms were evident (Fig. 4b). In the Pt_3Sn $L1_2$ superlattice structure, any Pt facets on the particle surface will likely have a layer of Sn atoms underneath. This may modify the Pt electronic properties so as to inhibit Pt oxidation in the 0.85 V region. A similar invariance of the Fourier transforms, and hence in the nearest neighbor interactions, have been observed previously in binary alloys of Pt with first row transition elements[20,21] and with Ru.[23] The Fourier transform of the Pt L_3 edge EXAFS for Pt/C with an upd Sn deposit (not shown) exhibited same spectra as Pt/C without upd Sn, an expected result since upd deposition was not expected to cause structural changes in the bulk of the crystallite.

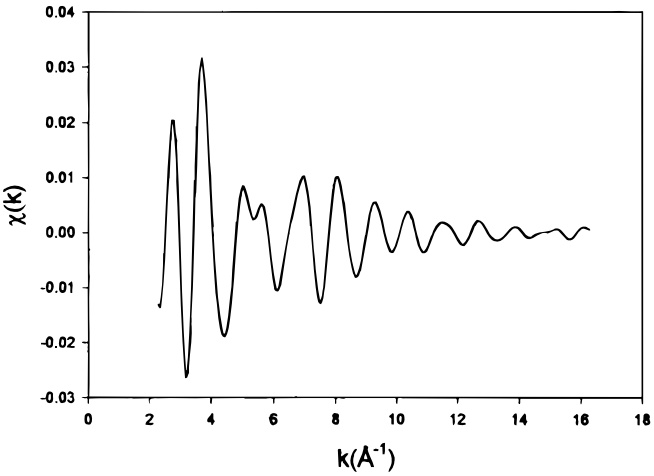

Figure 3. EXAFS at Pt L_3 edge for PtSn/C alloy at 0.0 V vs. RHE as a representative plot for data quality.

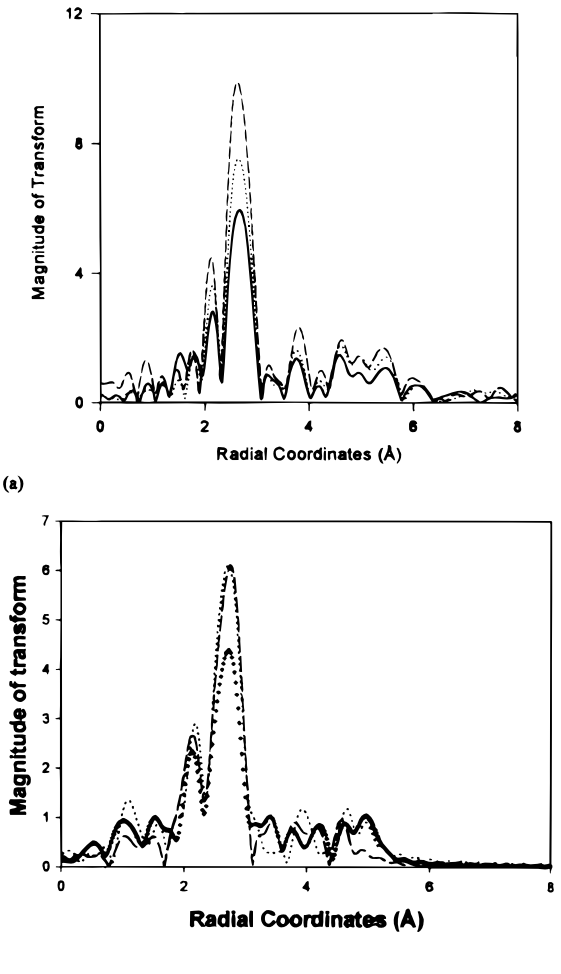

Figure 4. Forward Fourier transform of the EXAFS at Pt L_3 edge (k^3 weighted) in 1 M $HClO_4$ for (a) Pt/C at 0.0 (---), 0.54 (····), and 0.84 V (—) vs. RHE and (b) PtSn/C alloy at 0.0 (---), 0.54 (····), and 1.0 V (+) vs. RHE. Δk range given in Table III.

S0013-4651(97)10-113-6 CCC: $7.00

Table III. Fourier transformation ranges of the forward and inverse transforms (k^3 weighted) for Pt/C and PtSn/C electrocatalysts at 0.0, 0.54, and 0.84 V vs. RHE.

	0.0 V		0.54 V		0.84 V	
Electrocatalyst	Δk (Å^{-1})	Δr (Å)	Δk (Å^{-1})	Δr (Å)	Δk (Å^{-1})	Δr (Å)
Pt/C	3.53-14.31	1.41-3.41	3.49-14.23	1.40-3.05	3.20-15.03	1.30-3.04
PtSn/C	3.10-14.90	1.55-3.52	3.10-14.9	1.56-3.54	3.10-14.90	1.55-3.50

Fourier transformation ranges used in the forward and inverse transforms for reference standards.

Reference standard	Δk (Å^{-1})	Δr (Å)	N_{ref}	R_{ref}
Pt–Pt, Pt foil at 77 K	3.55-19.22	1.04-3.52	12	2.774
Pt–O, $Na_2Pt(OH)_6$, 77 K	3.52-17.18	1.05-2.40	6	2.052
Pt–Sn, FEFF program	2.56-19.24	1.50-3.51	12	2.829

Detailed analysis of the EXAFS at the Pt L_3 edge was performed after obtaining the inverse Fourier transforms, and performing fits with the appropriate phase and amplitude data. All fits were carried out using an iterative least square fitting.[36] The windows used for the inverse transforms for the sample are given in Table III. The relevant parameters for the forward, inverse transforms, bond distances, and coordination numbers used in the Pt-Sn FEFF theoretical calculations are also provided in Table III. The approach taken in fitting the sample data was to choose the simplest model first and attempt to get unique solutions to the fits. As reported previously[20] for Pt/C it was possible to fit the data to a single Pt-Pt coordination shell at both 0.0 and 0.54 V. At 0.84 V, single-shell fits were not adequate as has been shown before[20,21] and two shell fits with the Pt-Pt and Pt-O coordination shells provided best fits to the sample data. For the PtSn/C best fits to the sample data at 0.0, 0.54, and 0.84 V were obtained using a two-shell fit with the Pt–Pt and Pt–Sn coordination shells. The quality of fits for the PtSn/C alloy in 1 M $HClO_4$ at 0.54 V were excellent and are shown in Fig. 5 both for *k* and *r* space.

The results of the EXAFS analysis are given in Table II. For Pt/C, the primary perturbation to the structural characteristics as a function of potential appear as changes in the coordination number, with bond distances remaining unchanged. The higher coordination number at 0.0 V compared to 0.54 V can be accounted for on the basis of changes in the morphology of the particle from a more spherical shape at 0.0 V to a more raft-like structure at 0.54 V. This analysis has been described in more detail previously.[22] The bond distance and coordination number for the Pt–O interactions at 0.84 V are given in Table II, and this accounts for the further reduction of Pt–Pt coordination number compared to that at 0.54 V. In contrast to these, the PtSn/C alloy shows no changes in coordination number and bond distances (Pt–Pt and Pt–Sn). Increase in the Pt–Pt bond distance compared to Pt/C is evident and agrees with the XRD data. Evaluation of the particle size from coordination numbers for Pt/C at 0.0 V (spherical shape) and for PtSn/C (sum for Pt–Pt and Pt–Sn at any potential) shows good agreement with those obtained using XRD line broadening analysis. Correlation of coordination number to particle size was based on using an icosahedron cluster model and methodology developed by Benfield.[43] Further, the coordination number data for Pt–Pt and Pt–Sn are consistent with the presence of Pt_3Sn (Table II). The bond distances of 2.8 Å for both Pt–Pt and Pt–Sn are in good agreement with those reported by Meitzner et al. for PtSn on SiO_2.[26]

XAS at Sn K edge.—Figure 6a shows the Sn K edge XANES for the PtSn/C alloy in 1 M $HClO_4$ as a function of potential. Spectra for Sn, SnO, and SnO_2 are shown for comparison. The edge shift and the increase in the white line for the Sn K edge XANES in the alloy is probably due to a combination of the effect of alloying and the formation of oxidized Sn species on the electrocatalyst surface. Alloying causes the transfer of electrons from Sn to Pt involving the Sn 2 p states as well as change in the crystal symmetry in going from the tetragonal white Sn allotropic form to the fcc $L1_2$ structure, both of which contribute to the change in the XANES structure. However, changes in the spectra as a function of potential are undoubtedly due to the formation of oxidized Sn species or to changes in Sn–O coordination on the electrocatalyst surface. This was further confirmed using the Fourier transforms of the Sn K edge EXAFS.

The Fourier transform of the EXAFS at the Sn K edge in 1 M $HClO_4$ for PtSn/C alloy (Fig. 6b) shows peaks for Sn–Sn and Sn–Pt interactions (peak above 2 Å) as well as peaks for Sn–O interactions (peaks below 2 Å). The nature of the Sn–O interactions varies with potential as indicated by the coalescence of the two peaks, below

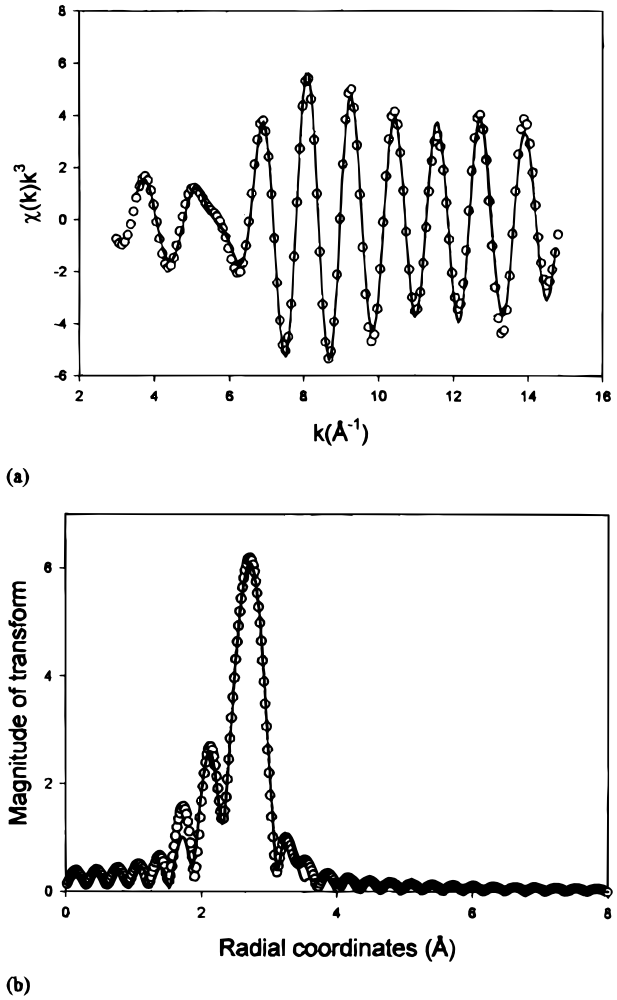

Figure 5. Two shell fit of the EXAFS spectra at Pt L_3 edge for PtSn/C at 0.54 V vs. RHE in 1 M $HClO_4$ in (a) k space and (b) r space. The fits are k^3 weighted with the sample data denoted by (○) and the fitted data by (—).

S0013-4651(97)10-113-6 CCC: $7.00

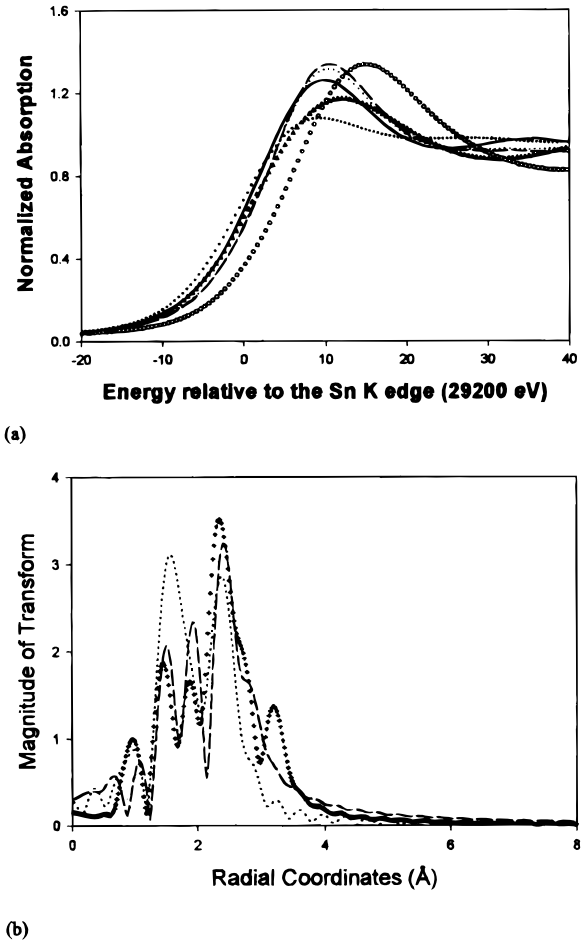

Figure 6. XAS at the Sn K edge in 1 M $HClO_4$ for PtSn/C alloy (a) XANES at 0.0 (—), 0.54 (····), and 0.84 V (---) V, data for Sn foil (+), SnO (△), and SnO_2 (°) are also shown; (b) forward Fourier transform (k^3 weighted) at 0.0 (---), 0.40 (+), and 0.54 (····) V. Δk = 3.0-12.5 $Å^{-1}$.

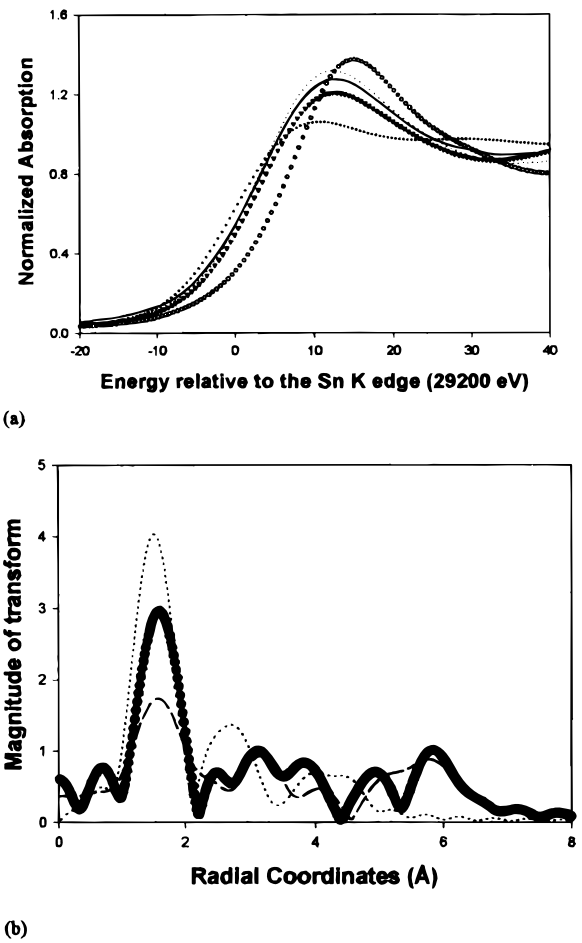

Figure 7. XAS at the Sn K edge for upd Sn on Pt/C in 0.5 M H_2SO_4: (a) XANES at 0.0 (—) and 0.54 (····) V, data for Sn foil (+), SnO (△) and SnO_2 (°) are also shown; (b) forward Fourier transform (k^3 weighted) at 0.0 (---), 0.24 (●), and 0.54 V (····) vs. RHE. Δk = 2.35 to 8.2 $Å^{-1}$.

2 Å, that are seen in the 0.0 to 0.4 V region, into one peak at 0.54 V. Since all the electrodes were optimized for Pt L_3 edge XAS, the step height at the Sn K edge was low. So the quality of EXAFS at the Sn K edge, for the PtSn/C alloy, did not permit detailed analysis. Furthermore, the Sn content was not dilute enough to permit fluorescence measurements. The Sn K edge EXAFS for the upd Sn on Pt/C in 0.5 M H_2SO_4 was obtained in fluorescence mode, yielding data of sufficient quality for EXAFS analysis.

Figure 7a shows the Sn K edge XANES spectra for the upd Sn in 0.5 M H_2SO_4. The spectra are similar to that for SnO except that the white line is more intense. The intensity of the white line increases reversibly with increasing potential. The change in the Sn K edge in going from Sn(II) to Sn(IV) is much greater than that found for Sn(0) to Sn(II), so up to 0.54 V there is no clear evidence for the formation of Sn(IV) species. Figure 7b shows the Fourier transforms as a function of potential. The Sn K edge EXAFS was highly attenuated, indicating weak bonding and a disordered adsorbed layer. This limited the integration range for the Fourier transform from 2.35 to 8.2 $Å^{-1}$. The intensity of the first EXAFS peak ~1.5 Å corresponding to the Sn–O interactions increases with potential. The effect is reversible with potential. No Sn–Pt interaction could be detected, presumably due to the disordered nature of the layer. Analysis of the first peak of the EXAFS, corresponding to the Sn–O interactions, is given in Table IV. The analysis reveals that the increase in the magnitude of the Sn–O interactions are due to a decrease in the Debye-Waller factor, rather than an increase in the coordination number. This was evident from the raw data, where the EXAFS oscillations ended at 7 $Å^{-1}$ at 0.0 V and at 10 $Å^{-1}$ at 0.54 V. The results indicate that the strength of the Sn–O interaction increases with increasing potential and that the Sn is associated with oxygenated species at all potentials. Perhaps, with increasing positive potentials, there is conversion from hydrated Sn^{2+}, to $Sn(OH)_x^{x-2}$, to hydroxides such as $Sn_6O_4(OH)_4$ [44] and finally to SnO like species. This could explain the apparent random changes in Sn–O bond distances. Presumably, it is these labile oxygen species that account for the electrocatalytic activity of upd Sn for the MOR and CO oxidation.

Discussion.—The XRD and XAS results indicate that alloying of Pt with Sn to form the Pt_3Sn fcc, $L1_2$ phase increases Pt–Pt bond distance and decreases 5 d band vacancies. The decrease in the Pt 5 d band vacancies can be viewed simplistically as a donation of electrons from the Sn 5 p and s bands to the Pt 5 d band, which is a pow-

Table IV. Results of EXAFS analysis at the Sn K edge for upd Sn on Pt/C in 1 M $HClO_4$ showing magnitude of the various EXAFS parameters for the Sn–O interactions.

Electrode potential (V vs. RHE)	EXAFS parameters for Sn–O shell			
	N	R (Å)	$\Delta\sigma^2$ ($Å^2$)	ΔE_0 (mV)
0.54	6.0	2.05	0.0004	5.1
0.39	4.6	2.09	0.0001	0.0
0.24	3.5	2.10	−0.070	0.0
0.15	5.2	2.04	0.0020	5.7
0.0	4.8	2.10	0.0080	0.5

S0013-4651(97)10-113-6 CCC: $7.00

erful acceptor. Electron donation by Sn to Pt agrees with the molecular orbital calculations of Anderson.[45] These calculations, based on substitutional Sn atoms on a Pt <111> surface in a $Pt_{17}Sn$ cluster model, also imply that Sn, despite its electron donation to Pt, is not a strong acceptor of electrons from water molecules and as a result Sn should form weak bonds with OH^-. The present results indicate that both upd Sn and surface Sn in alloyed Sn interact with oxygen species at all potentials. Analysis of the Sn EXAFS for upd Sn on Pt/C clearly indicates that Sn interacts with oxygen species at all potentials and that there is an increase in the strength of the Sn–O bond at more positive potentials. Sn XANES for the PtSn/C alloy electrocatalyst also indicate Sn–O interactions, and inspection of the Fourier transforms of the EXAFS also show changes in the Sn–O interactions at more positive potentials. There is no clear evidence for Sn(IV) formation in the normal potential region for CO or methanol oxidation. These observations agree in part with those previously reported by Sobkowski et al.,[46] who suggested in the case of adsorbed Sn the Sn is adsorbed more as a divalent ion rather than as a metallic-like adatom.

XAS at the Pt L edges indicates that upd Sn on Pt/C has minimal effects on both the Pt d band vacancies and the short range atomic order of the Pt, so Pt remains largely unchanged both electronically as well as structurally. Hence, the principal difference between the alloyed and the upd-deposited Sn is the major effects of alloyed Sn on both the electronic and structural environment around the Pt atoms. The increased Pt–Pt bond distance and the lower Pt d band vacancies result in an unfavorable environment for the initial adsorption and abstraction of the first C–H bond for the start of methanol oxidation. The situation is different in the case of upd Sn on Pt/C. Since the structural and electronic properties of Pt atoms remain unchanged, the adsorption step and the abstraction of the C–H bond in the initial methanol oxidation step proceeds in a similar fashion as on Pt/C. The oxygenated species on the upd Sn atoms at lower potentials are then able to initiate the oxidation of CO and CHO moieties as they are formed. In the case of CO oxidation the adsorbed oxygenated species on the Sn in PtSn/C can promote CO oxidation at low potentials, hence the enhanced activity for CO oxidation.

Part II of this paper presents in situ XAS results for PtSn/C, and Pt/C with upd Sn both in the presence of adsorbed CO and under conditions of methanol oxidation.

Conclusions

This paper examines the effect of potential on the electronic and structural characteristics of Pt and Sn when Sn is either alloyed with Pt or is present as upd deposits on the carbon-supported Pt. Alloying of Sn with Pt in a 3:1 ratio results in the formation of a Pt_3Sn $L1_2$ phase, a decrease in the Pt d band vacancies, an increase in the lattice parameters, and hence larger Pt–Pt bond distances. These changes are opposite to the effect of alloying Pt with first row transition metal elements or with Ru, where there are increases in the d band vacancies and contractions in the lattice parameters. Deposition of Sn as upd adatoms on Pt/C has minimal effects on the electronic or structural aspects of Pt/C. Both upd Sn on Pt/C and Sn surface atoms in the PtSn/C alloy are similar in that both exhibit Sn-oxygen interactions that vary with potential. The Sn atoms in both upd Sn on Pt/C and in PtSn/C catalysts are associated with oxygenated species and as a result can initiate the oxidation of adsorbed CO and CHO at lower potentials as compared to Pt/C. The main differences in the catalytic activity of PtSn/C and upd Sn on Pt/C for methanol oxidation is due to the differences in the electronic properties of the Pt in these catalysts. The upd Sn does not interfere with the ability of the Pt to adsorbed methanol and dissociate C–H bonds, whereas alloying with Sn inhibits the ability of Pt to carry out these functions. This provides important pointers for explaining the different activities exhibited by alloyed PtSn/C and upd Sn on Pt/C for methanol oxidation.

Acknowledgments

The authors gratefully acknowledge the support of the Assistant Secretary for Energy Efficiency and Renewable Energy, Office of Transportation Technologies, Electric and Hybrid Vehicles, USDOE, under contract no. DE-AC02-98CH10886.

The authors gratefully acknowledge support of the USDOE, Division of Material Sciences, under contract no. DE-FG05-89ER45384 for its role in the development and operation of Beam line X11A at the National Synchrotron Light Source (NSLS). The NSLS is supported by the Department of Energy, Division of Material Science, under contract no. DE-AC02-98CH10886.

Brookhaven National Laboratory assisted in meeting the publication costs of this article.

References

1. B. D. McNicol, *J. Electroanal. Chem.*, **118**, 71 (1981).
2. B. D. McNicol, in *Power Sources for Electric Vehicles*, B. D. McNicol and D. A. J. Rand, Editors, pp. 807-838, Elsevier, Amsterdam (1984).
3. J.-M. Léger and C. Lamy, *Ber. Bunsenges, Phys. Chem.*, **94**, 1021 (1990).
4. R. Parsons and T. Vandernoot, *J. Electroanal. Chem.*, **257**, 9 (1988).
5. K. Cathro, *J. Electrochem. Soc.*, **116**, 1608 (1969).
6. (a) M. M. P. Janssen and J. Moolhuysen, *J. Catal.*, **46**, 289 (1977); (b) M. M. P. Janssen and J. Moolhuysen, *Electrochim. Acta*, **21**, 861 (1976).
7. M. R. Andrew, J. S. Drury, B. D. McNicol, C. Pinington, and R. T. Short, *J. Appl. Electrochem.*, **6**, 99 (1976).
8. A. A. Mikhailova, N. V. Ostrova, and Y. V. Vasil'ev, *Electrokhimiya*, **13**, 518 (1977).
9. B. Bittens-Cattaneo and T. Iwasita, *J. Electroanal. Chem.*, **238**, 151 (1987).
10. C. T. Hable and M. S. Wrighton, *Langmuir*, **7**, 1305 (1991).
11. M. Watanabe, Y. Furuchi, and S. Motoo, *J. Electroanal. Chem.*, **191**, 367 (1985).
12. A. Haner and P. N. Ross, Jr., *J. Phys. Chem.*, **95**, 3740 (1991).
13. K. Wang, H. A. Gasteiger, N. M. Markovic, and P. N. Ross, Jr., *Electrochim. Acta*, **41**, 2587 (1996).
14. S. A. Campbell and R. Parsons, *J. Chem. Soc., Faraday Trans.*, **88**, 833 (1992).
15. A. S. Arico, V. Antonucci, N. Giordano, A. K. Shukla, M. K. Ravikumar, A. Roy, S. R. Barman, and D. D. Sarma, *J. Power Sources*, **50**, 295 (1994).
16. H. A. Gasteiger, N. M. Markovic, and P. N. Ross, Jr., *J. Phys. Chem.*, **99**, 8945 (1995).
17. T. Iwasita and W. Vielstich, *J. Electroanal. Chem.*, **201**, 403 (1986).
18. J. Munk, P. A. Christensen, A. Hamnett, and E. Skou, *J. Electroanal. Chem.*, **401**, 215 (1996).
19. M. Watanabe and S. Motoo, *J. Electroanal. Chem.*, **60**, 275 (1975).
20. S. Mukerjee, S. Srinivasan, M. P. Soriaga, and J. McBreen, *J. Electrochem. Soc.*, **142**, 1409 (1995).
21. S. Mukerjee, S. Srinivasan, M. P. Soriaga, and J. McBreen, *J. Phys. Chem.*, **99**, 4577 (1995).
22. S. Mukerjee and J. McBreen, *J. Electrochem. Soc.*, **143**, 2285 (1996).
23. J. McBreen and S. Mukerjee, *J. Electrochem. Soc.*, **142**, 3399 (1995).
24. D. Aberdam, R. Durand, R. Faure, F. Gloaguen, J. L. Hazemann, E. Herrero, A. Kabbabi, and O. Ulrich, *J. Electroanal. Chem.*, **398**, 43 (1995).
25. S. Mukerjee and J. McBreen, *J. Electroanal. Chem.*, **448**, 163 (1998).
26. G. Meitzner, G. H. Via, F. W. Lytle, S. C. Fung, and J. H. Sinfelt, *J. Phys. Chem.*, **92**, 2925 (1988).
27. T. Inoue, K. Tomishige, and Y. Iwasawa, *J. Chem. Soc., Faraday Trans*, **92**, 461 (1996).
28. A. Borgna, S. M. Stagg, and D. Rescasco, *J. Phys. Chem. B*, **102**, 5077 (1998).
29. T. R. Thurston, N. M. Jisrawi, S. Mukerjee, X. Q. Yang, J. McBreen, and M. L. Daroux, and X. K. Xing, *Appl. Phys. Lett.*, **69**, 194 (1996).
30. J. McBreen, *J. Electroanal. Chem.*, **357**, 373 (1993).
31. J. Wong, F. W. Lytle, R. P. Messner, and D. H. Maylott, *Phys. Rev. B*, **30**, 5596 (1984).
32. A. N. Mansour, J. W. Cook, Jr., and D. E. Sayers, *J. Chem. Phys.*, **88**, 2330 (1984).
33. A. N. Mansour, J. W. Cook, Jr., D. E. Sawyers, R. J. Emrich, and J. R. Katzer, *J. Catal.*, **89**, 464 (1984).
34. J. B. A. D. van Zon, D. C. Koningsberger, H. F. J. vant'Blik, and D. E. Sayers, *J. Chem. Phys.*, **82**, 5742 (1985).
35. F. B. M. Duivenvoorden, D. C. Koningsberger, Y. S. Oh, and B. C. Gates, *J. Am. Chem. Soc.*, **108**, 6254 (1986).
36. P. H. Citrin, P. Eisenberger, and B. M. Kincaid, *Phys. Rev. Lett.*, **36**, 1346 (1976).
37. J. J. Rehr. J. Mustre de Leon, S. I. Zabinski, and R. C. Albers, *J. Am. Chem. Soc.*, **113**, 5135 (1991).
38. D. C. Koningsberger, in *Synchrotron Techniques in Interfacial Electrochemistry*, C. A. Melendres and A. Tadjeddine, Editors, pp. 181-198, Kluwer Academic Publishers, Dorddrecht (1994).
39. JCPDS-ICDD, 35-1360 (1995).
40. W. Pearson, *Handbook of Lattice Spacing and Structure of Metals and Alloys*, Vol. 4, Pergamon Press, New York (1988).
41. W. H. McMaster, N. Kerr del Grande, J. H. Mallet, and J. H. Hubbel, *Compilation of X-Ray Cross Sections*, National Technical Information Service, Springfield, VA (1969).
42. G. H. Via, J. H. Sinfelt, and F. W. Lytle, *J. Chem. Phys.*, **71**, 690 (1979).
43. R. E. Benfield, *J. Chem. Soc., Faraday Trans.*, **88**, 1107 (1992).
44. A. F. Wells, *Structural Inorganic Chemistry*, 5th ed., p. 1186, Clarendon Press, Oxford (1993).
45. A. B. Anderson, E. Grantscharova, and P. Schiller, *J. Electrochem. Soc.*, **142**, 1880 (1995).
46. J. Sobkowski, K. Franaszczuk, and A. Piasecki, *J. Electroanal. Chem.*, **196**, 145 (1985).